

## One-step rapid synthesis of $\pi$ -conjugated large oligomers *via* C–H activation coupling

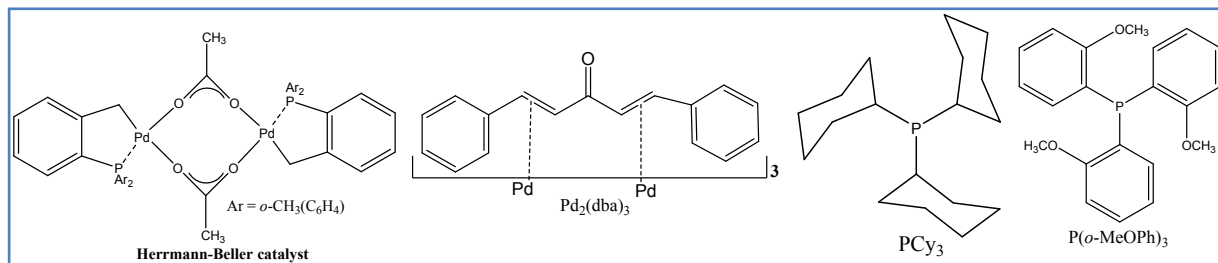
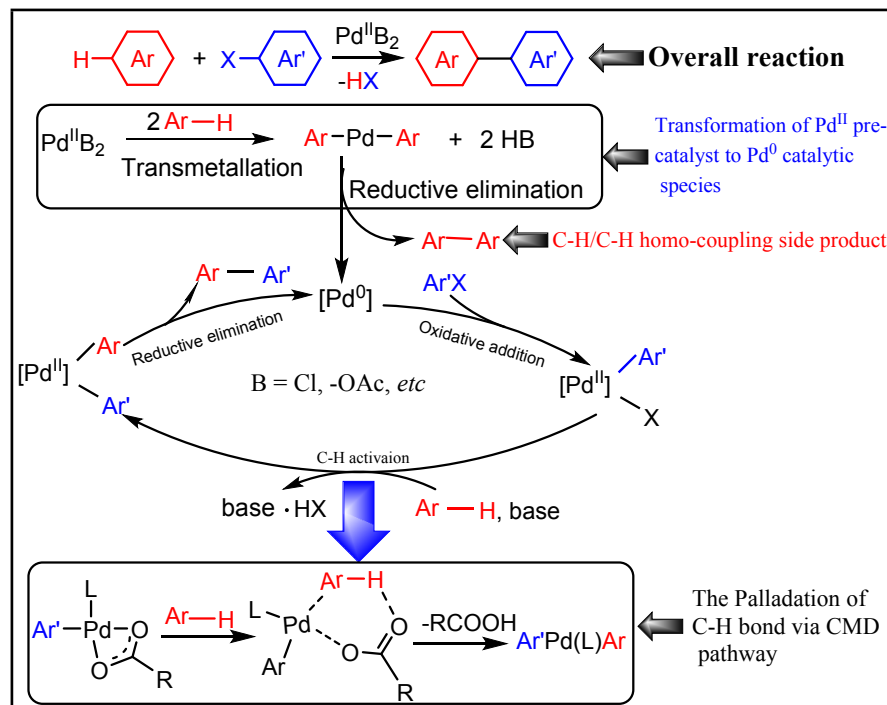
Shi-Yong Liu,<sup>\*ab</sup> Di-Gang Wang,<sup>b</sup> Ai-Guo Zhong<sup>b</sup> and He-Rui Wen<sup>\*a</sup>

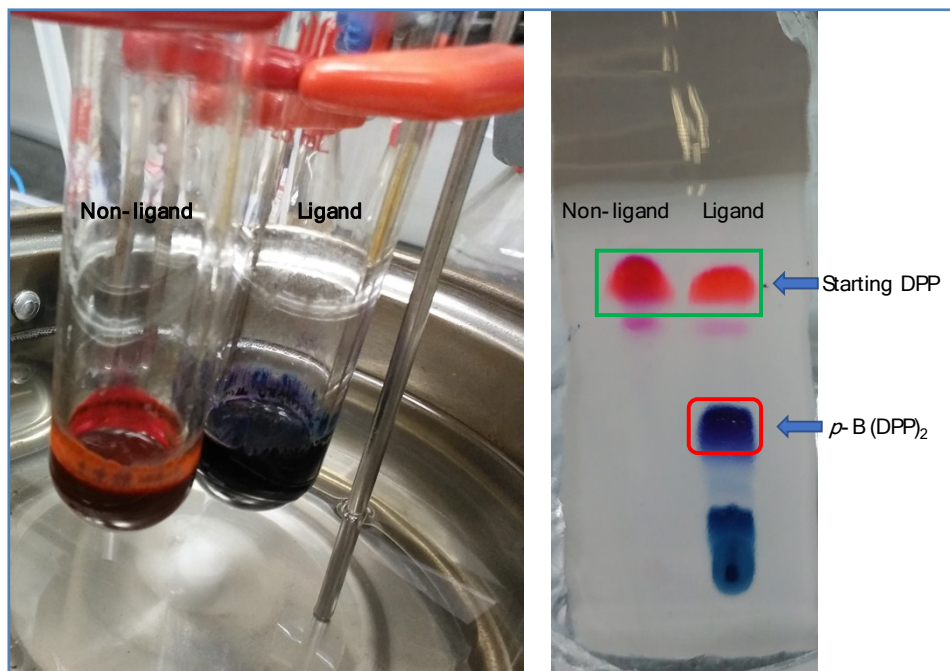
<sup>a</sup>School of Metallurgical and Chemical Engineering, Jiangxi University of Science and Technology, Ganzhou 341000, P. R. China

<sup>b</sup>Department of Pharmacy & Chemistry, Taizhou University, Taizhou 317000, P. R. China

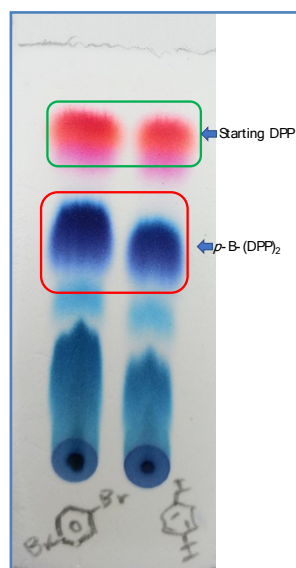
### Contents

1. Figs. S1 .....	S2
2. Scheme S1.....	S2
3. Fig. S2 and 3.....	S3
4. Fig. S4 .....	S4
5. Fig. S5.....	S5
6. Fig. S6.....	S6
7. Fig. S7 .....	S7
8. $^1\text{H}$ and $^{13}\text{C}$ NMR, and Maldi-TOF MS spectra.....	S8-22

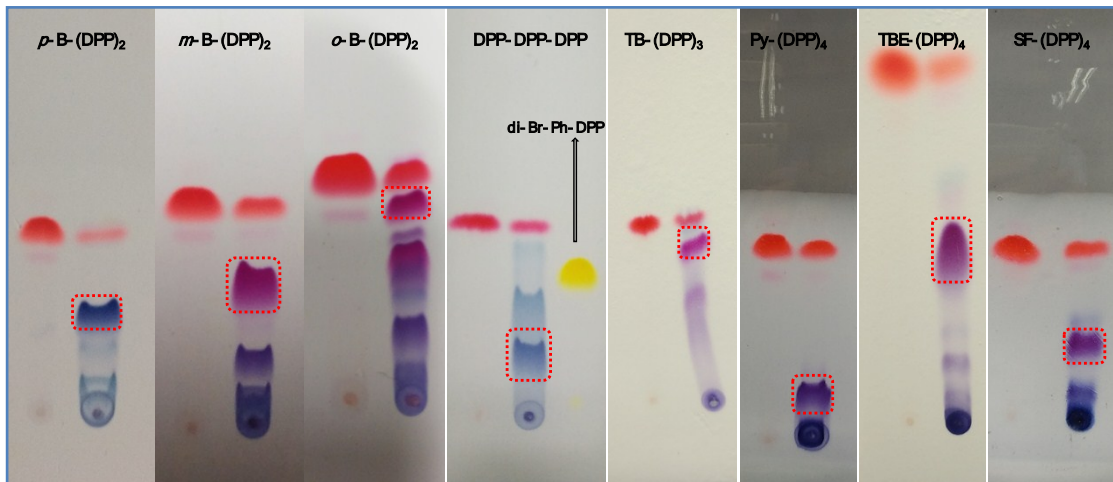
**Fig. S1** The molecular structures of Herrmann-Beller catalyst,  $\text{Pd}_2(\text{dba})_3$ ,  $\text{PCy}_3$  and  $\text{P}(\text{o-MeOPh})_3$ .**Scheme S1** The Pd-catalyzed DA reaction, the reduction of  $\text{Pd}^{\text{II}}$  pre-catalyst to  $\text{Pd}^0$  catalytic species, the catalytic cycle of the DA coupling, and the palladation of C-H bond.



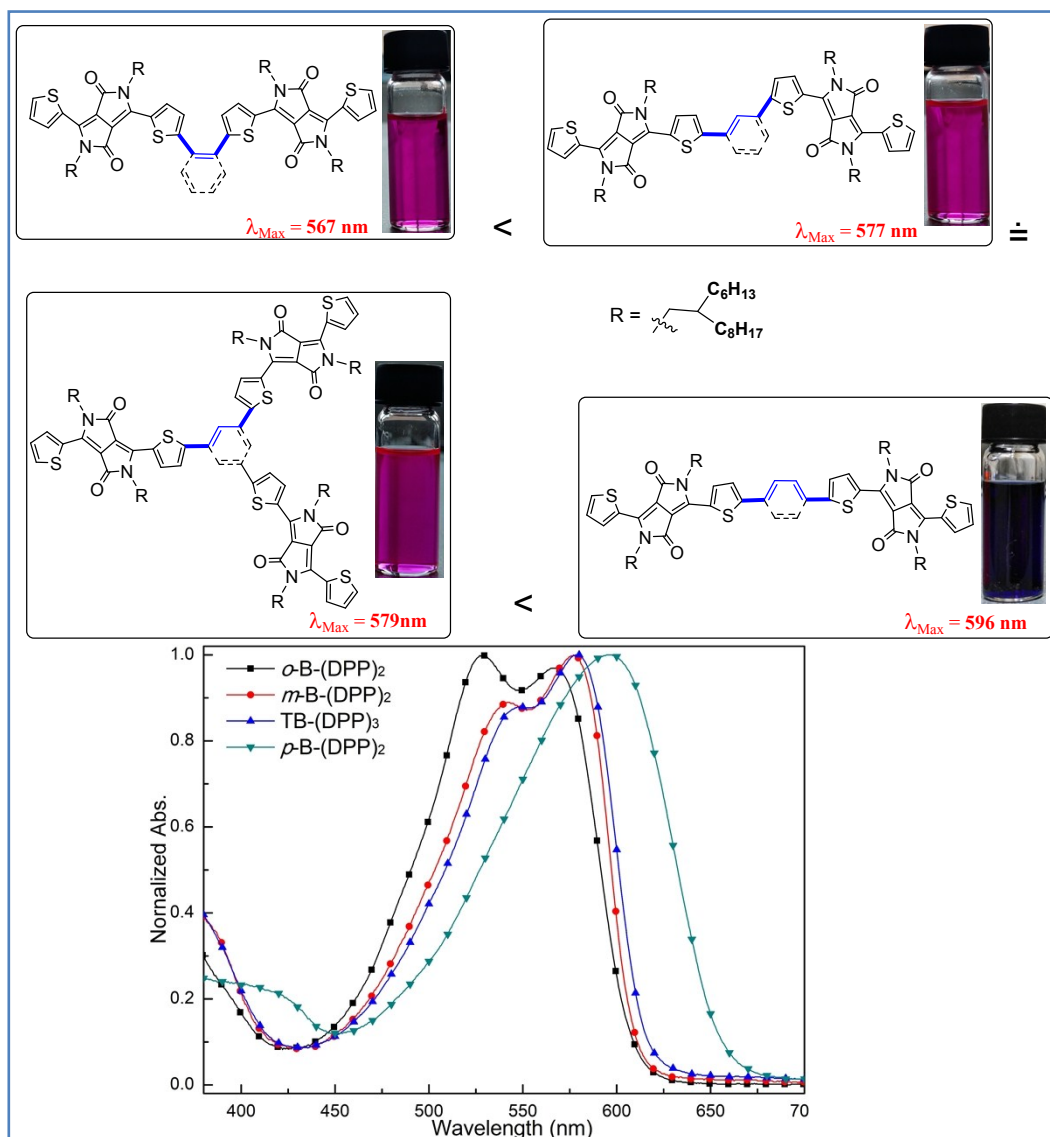
**Fig. S2** The reaction between DPP and *p*-dibromobenzene with and without ligand  $P(o\text{-MeOPh})_3$  using toluene as reaction medium (entries 10 and 11 in Table 1). Digital photos of (a) The reaction mixtures after reacting for 12 h and cooling to room temperature. (b) The TLC analysis of both reaction mixtures, using  $\text{CH}_2\text{Cl}_2$  : hexane (2:1, v/v) as eluent, and the spots marked with green and red frame are the reactant DPP and target product  $p\text{-B(DPP)}_2$ , respectively.



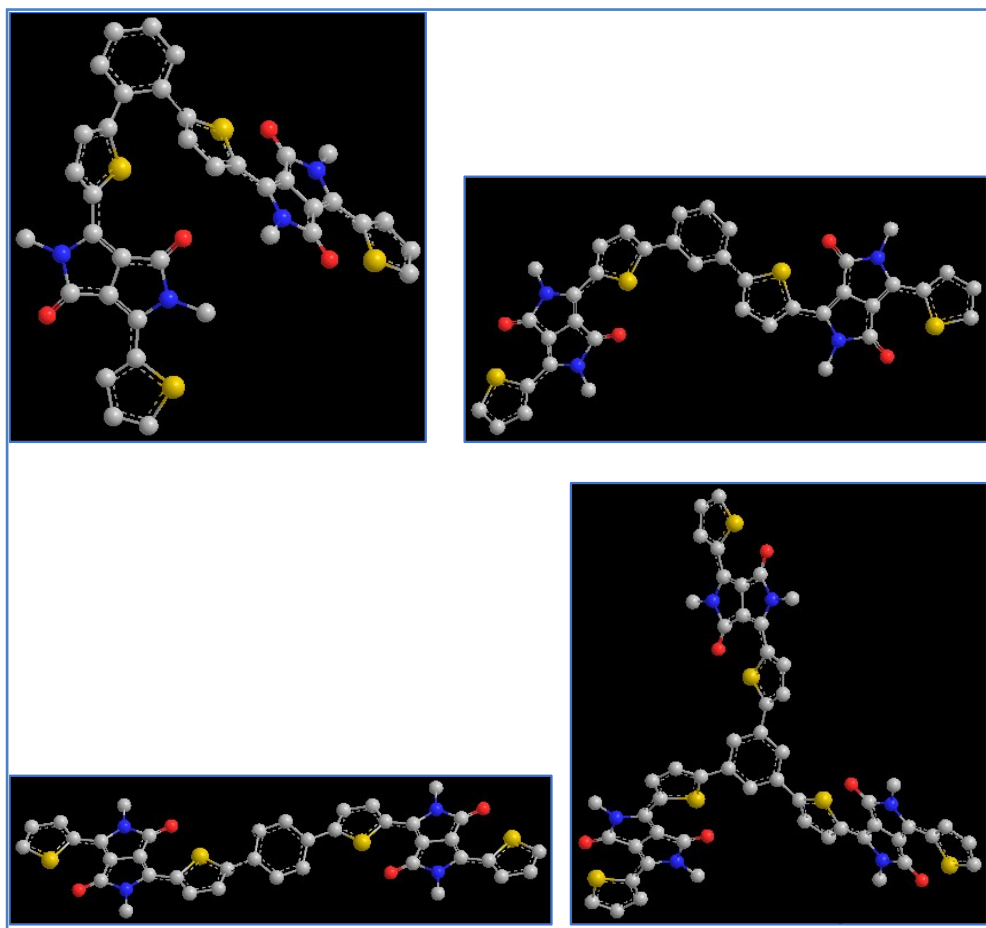
**Fig. S3** The TLC analysis of the reactions between DPP and *p*-dibromobenzene (left) or *p*-diiodobenzene (right). (see Entries 12 and 13 in Table 1). The spots marked with green and red frame are the reactant DPP and target product  $p\text{-B(DPP)}_2$ , respectively.



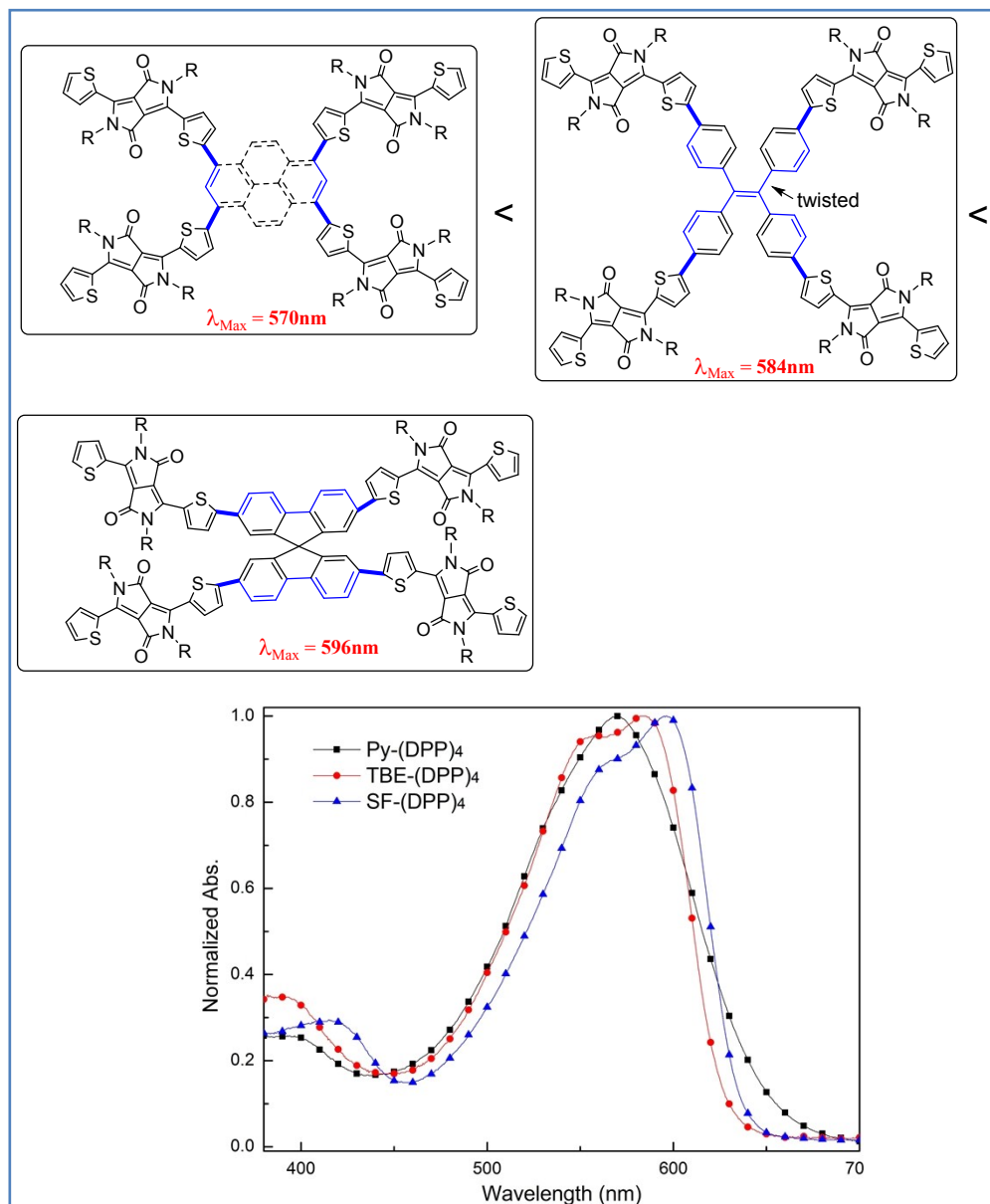
**Fig. S4** Digital photos of TLC analysis of the synthetic reactions for the eight oligomers. From left to right are respectively *p*-B-(DPP)<sub>2</sub>, *m*-B-(DPP)<sub>2</sub>, *o*-B-(DPP)<sub>2</sub>, DPP-DPP-DPP, TB-(DPP)<sub>3</sub>, Py-(DPP)<sub>4</sub>, TBE-(DPP)<sub>4</sub> and SF-(DPP)<sub>4</sub>. For all the TLC plates, the spots on the left are the starting DPP, and the spots marked with red dotted frames are the target oligomers.



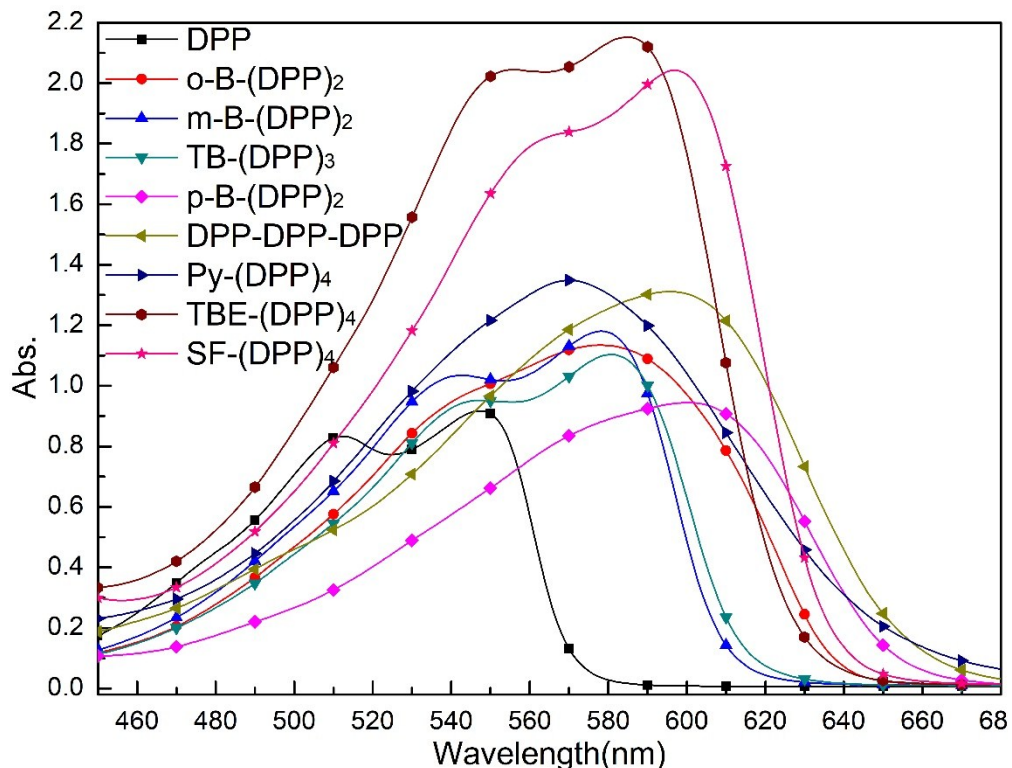
**Fig. S5** The shortest pathways of  $\pi$ -electron delocalization (marked with blue color) of the phenyl-cored DPP-based oligomers ***o***-B-(DPP)<sub>2</sub>, ***m***-B-(DPP)<sub>2</sub>, ***p***-B-(DPP)<sub>2</sub> and TB-(DPP)<sub>3</sub>, and the corresponding normalized Uv-vis spectra (below).



**Fig. S6** DFT optimized geometries of phenyl-cored DPP-based oligomers, *o*-B-(DPP)<sub>2</sub>, *m*-B-(DPP)<sub>2</sub>, *p*-B-(DPP)<sub>2</sub> and TB-(DPP)<sub>3</sub> (the alkyl chains replaced by methyl groups).



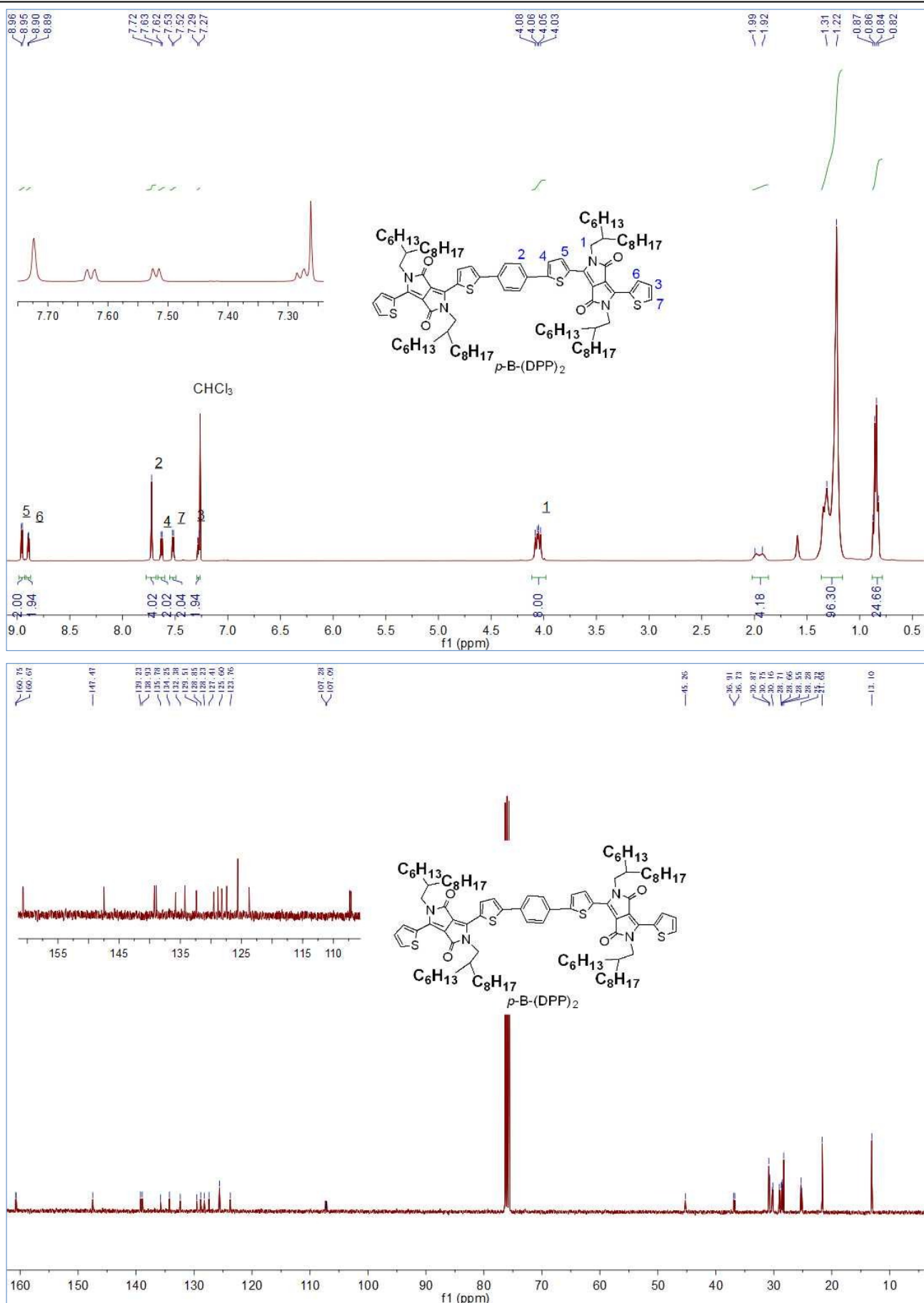
**Fig. S7** The shortest pathways of  $\pi$ -electron delocalization (marked with blue color) of the **Py-**, **TBE-** and **SF-(DPP)<sub>4</sub>** oligomers, and the corresponding normalized Uv-vis spectra (below).

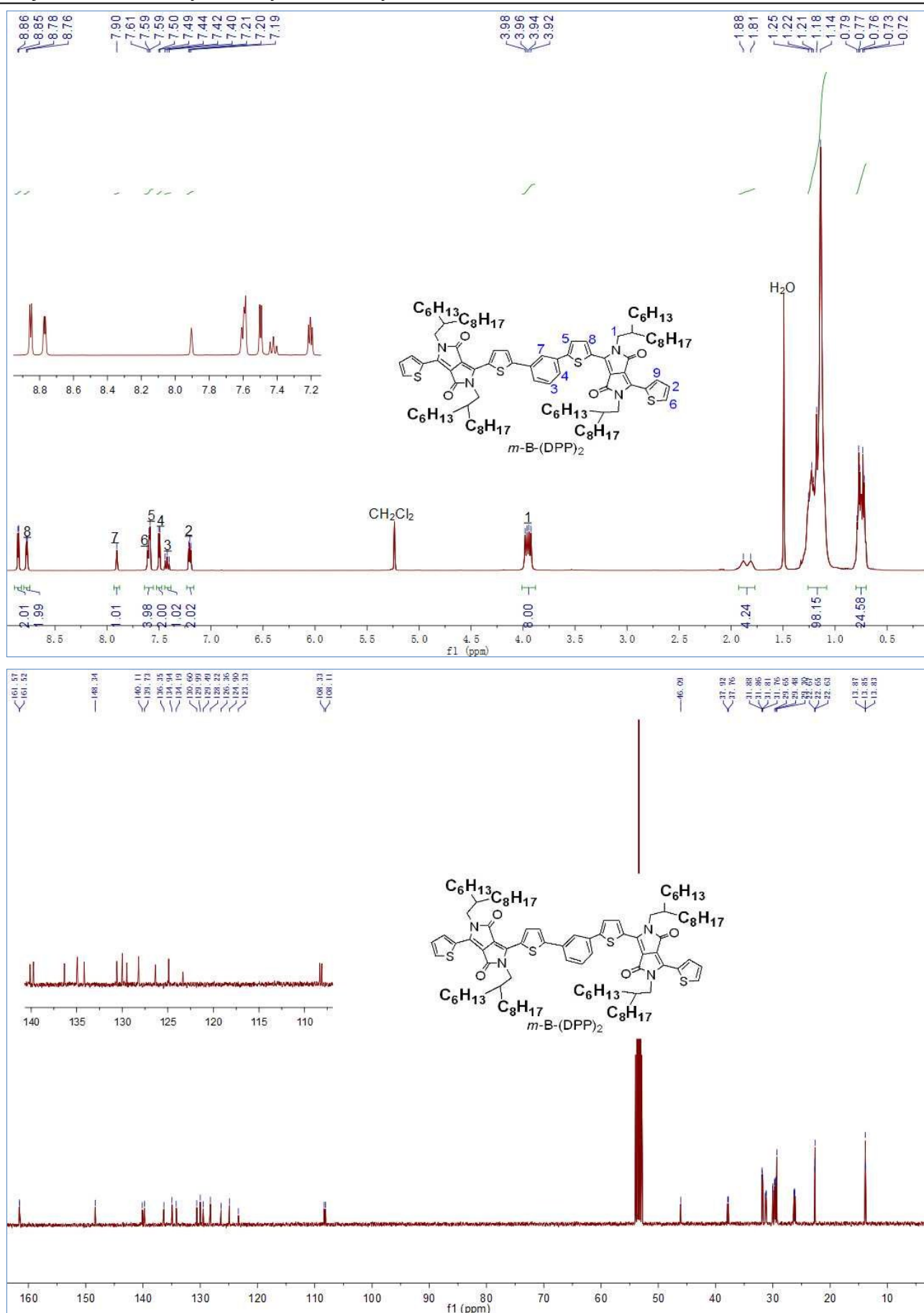


**Fig. S8** The Uv-vis spectra of the starting DPP, oligomers *o*-B-(DPP)<sub>2</sub>, *m*-B-(DPP)<sub>2</sub>, TB-(DPP)<sub>3</sub>, *p*-B-(DPP)<sub>2</sub>, Py-(DPP)<sub>4</sub>, TBE-(DPP)<sub>4</sub> and SF-(DPP)<sub>4</sub> in CHCl<sub>3</sub> at concentrations of 4.54, 2.54, 2.03, 1.55, 2.16, 1.89, 1.07, 1.69 and  $1.27 \times 10^{-5}$  mol/L.

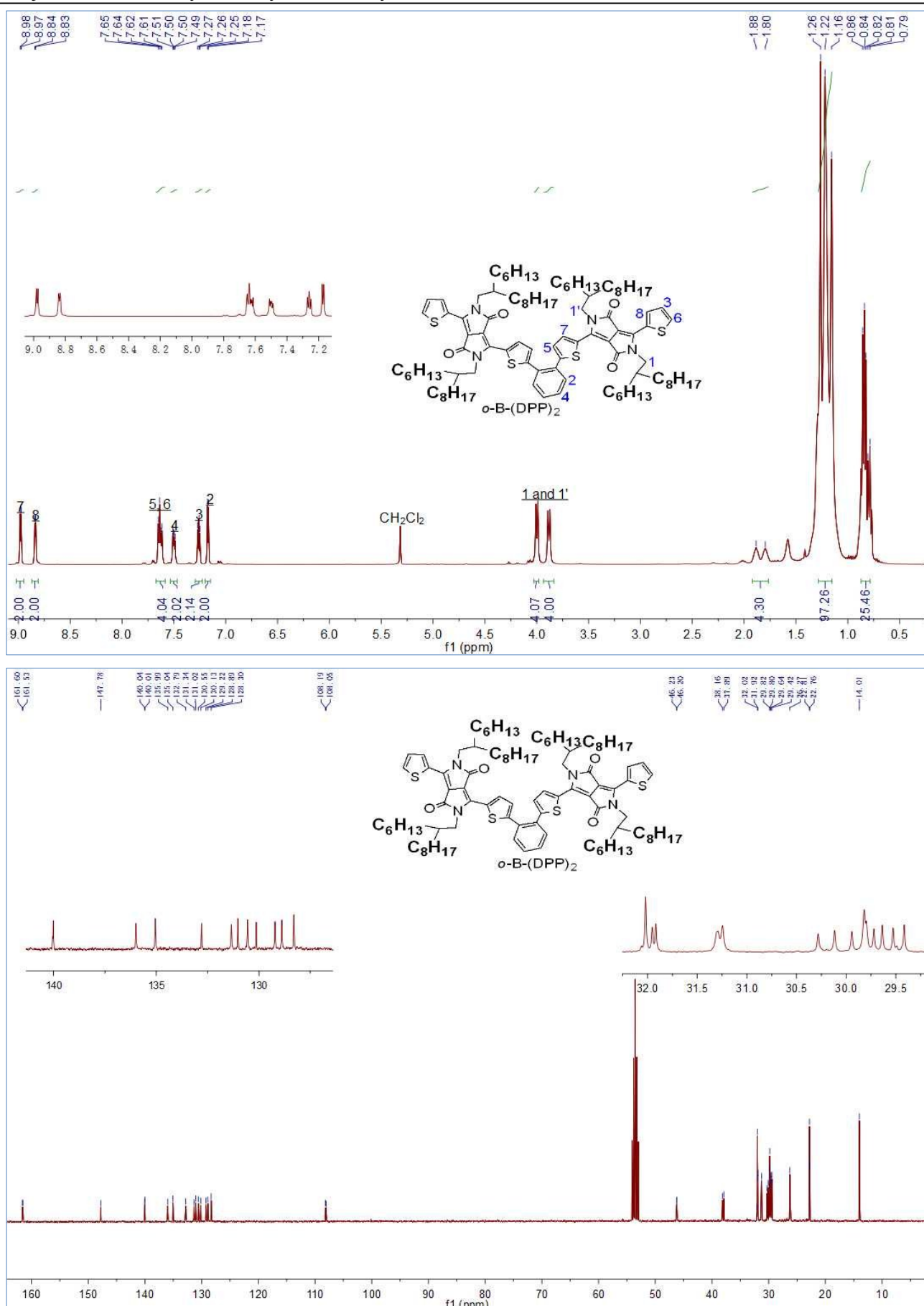
**Table S1** The extinction coefficients of the DPP materials at  $\lambda_{\text{max}}$  ( $\times 10^4$  M<sup>-1</sup> cm<sup>-1</sup>).

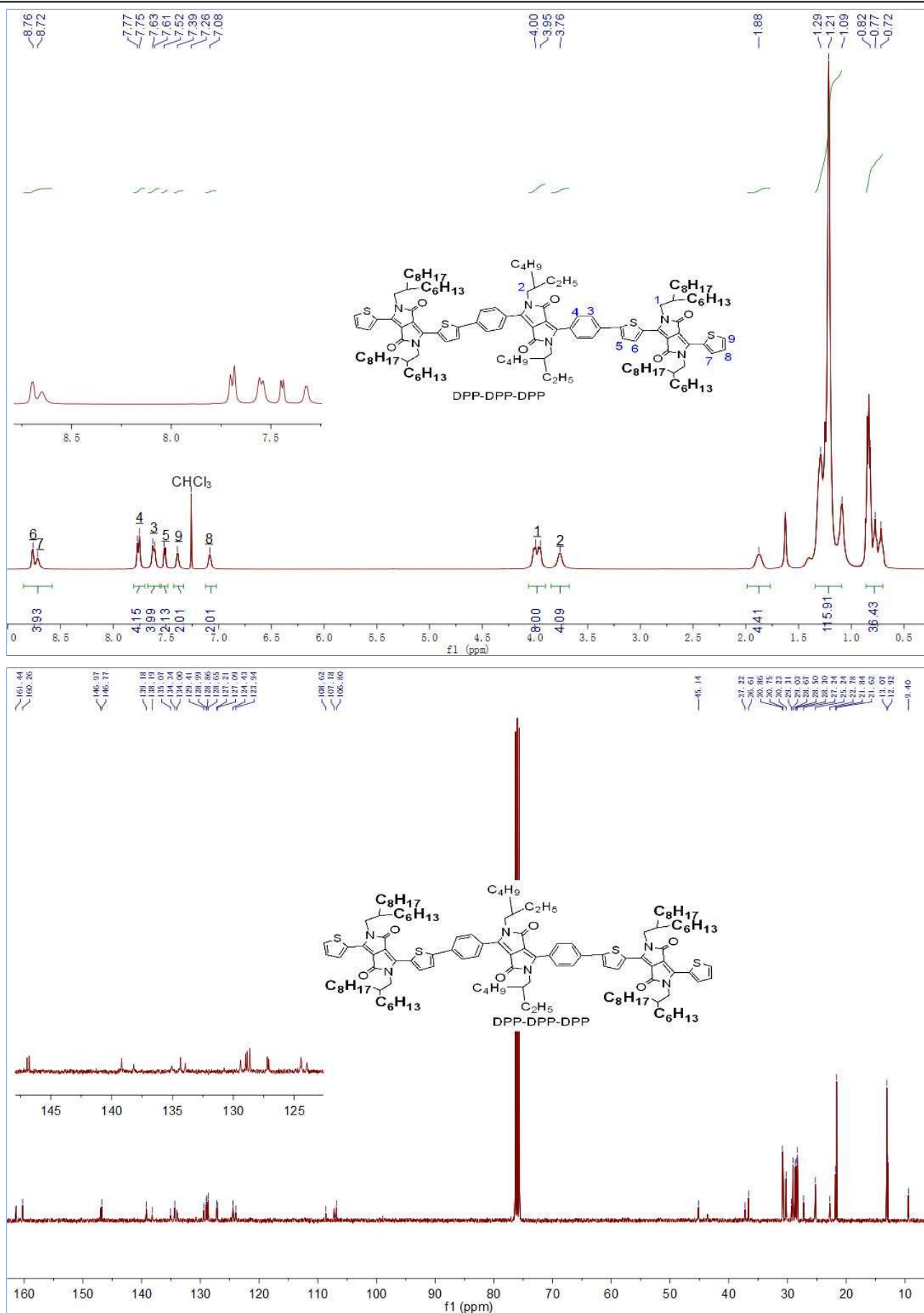
DPP	<i>o</i> -B-(DPP) <sub>2</sub>	<i>m</i> -B-(DPP) <sub>2</sub>	<i>p</i> -B-(DPP) <sub>2</sub>	TB-(DPP) <sub>3</sub>	DPP-DPP-DPP	Py-(DPP) <sub>4</sub>	TBE-(DPP) <sub>4</sub>	SF-(DPP) <sub>4</sub>
2.02	4.47	5.82	4.38	6.94	7.12	12.61	12.74	14.08

**Fig. S8** The <sup>1</sup>H and <sup>13</sup>C NMR spectra of *p*-B-(DPP)<sub>2</sub> in  $\text{CDCl}_3$ .

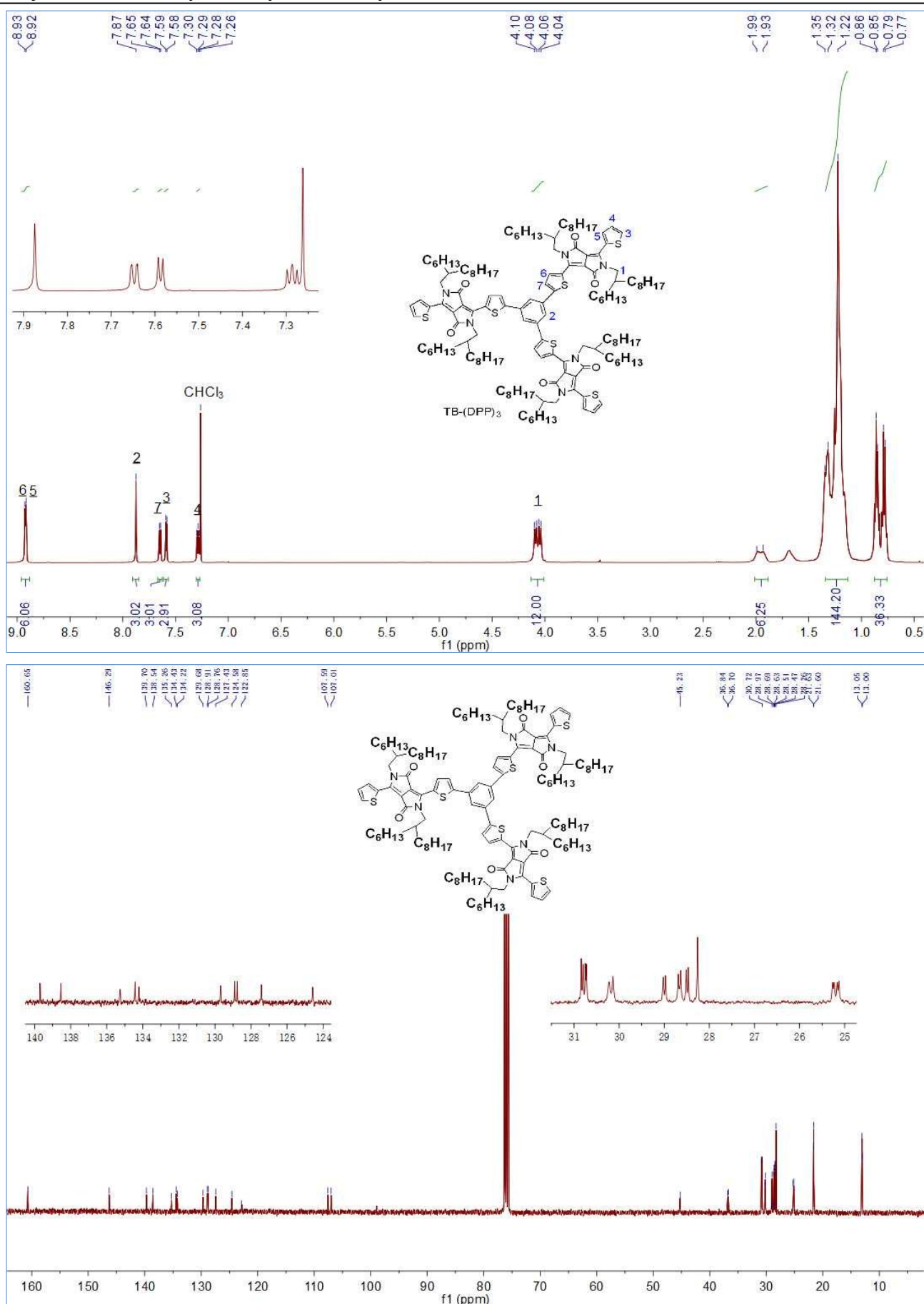


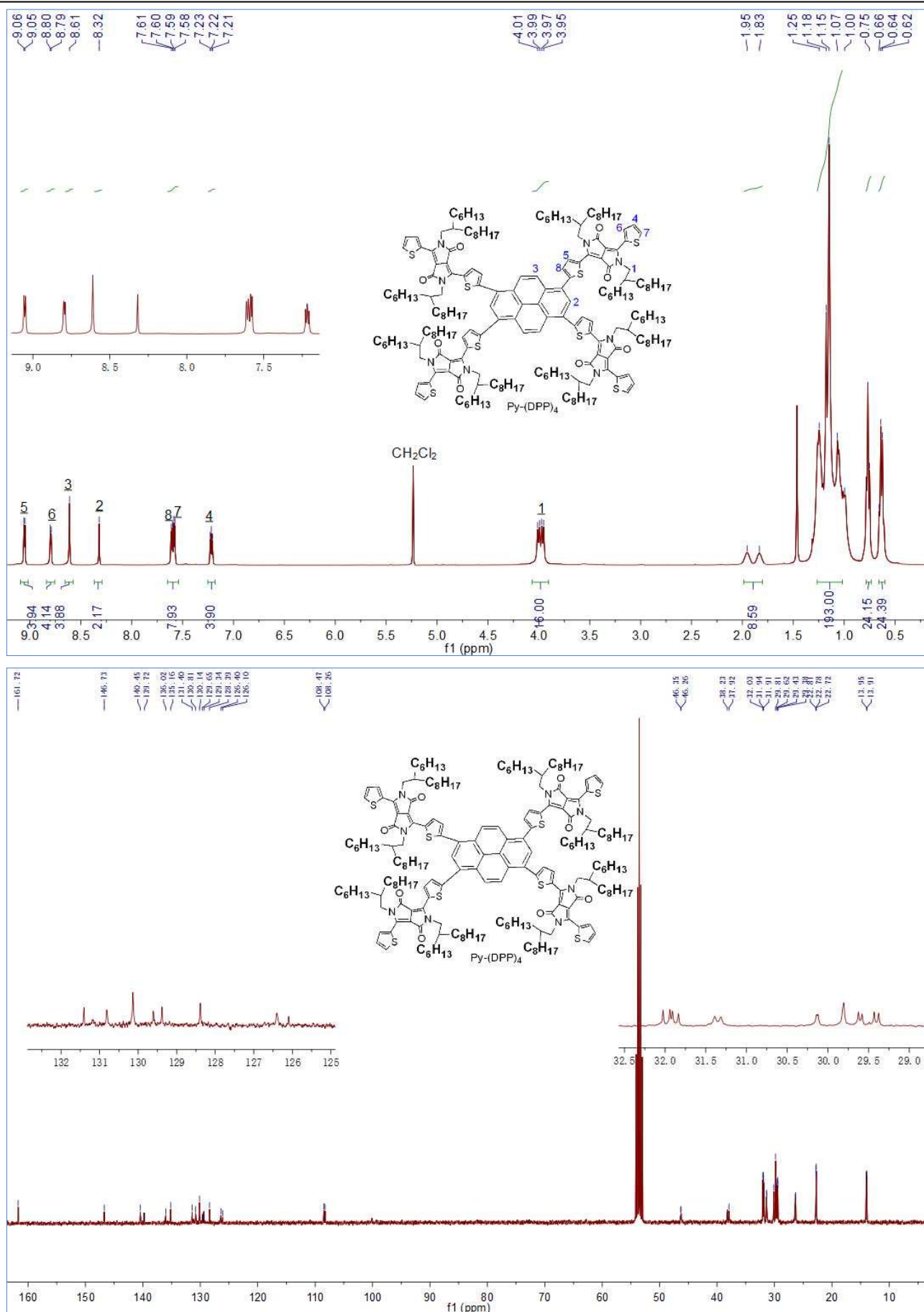
**Fig. S9** The  $^1\text{H}$  and  $^{13}\text{C}$  NMR spectra of **m-B-(DPP)<sub>2</sub>** in  $\text{CD}_2\text{Cl}_2$ .

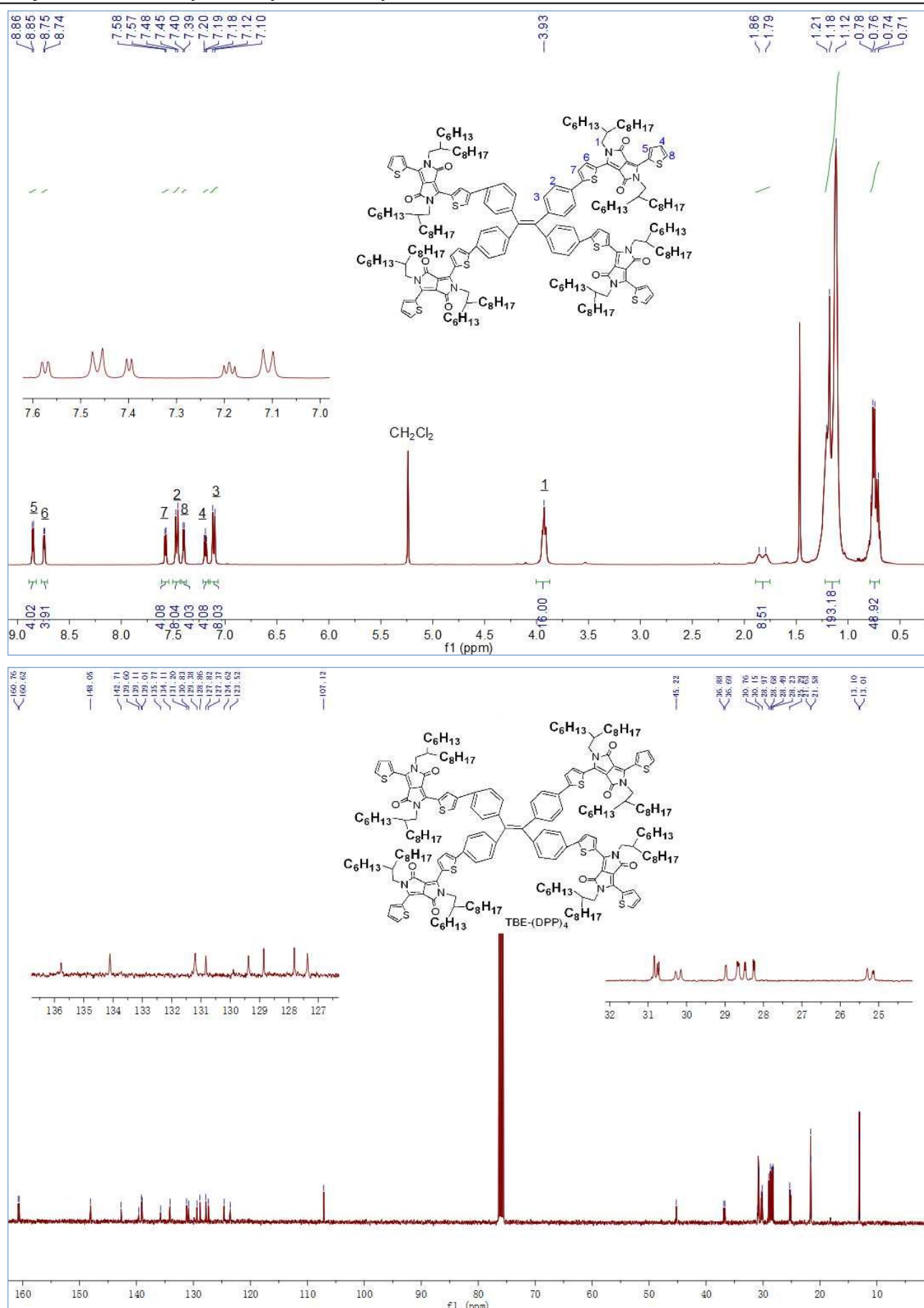
**Fig. S10** The  $^1\text{H}$  and  $^{13}\text{C}$  NMR spectra of *o*-B-(DPP)<sub>2</sub> in  $\text{CD}_2\text{Cl}_2$ .

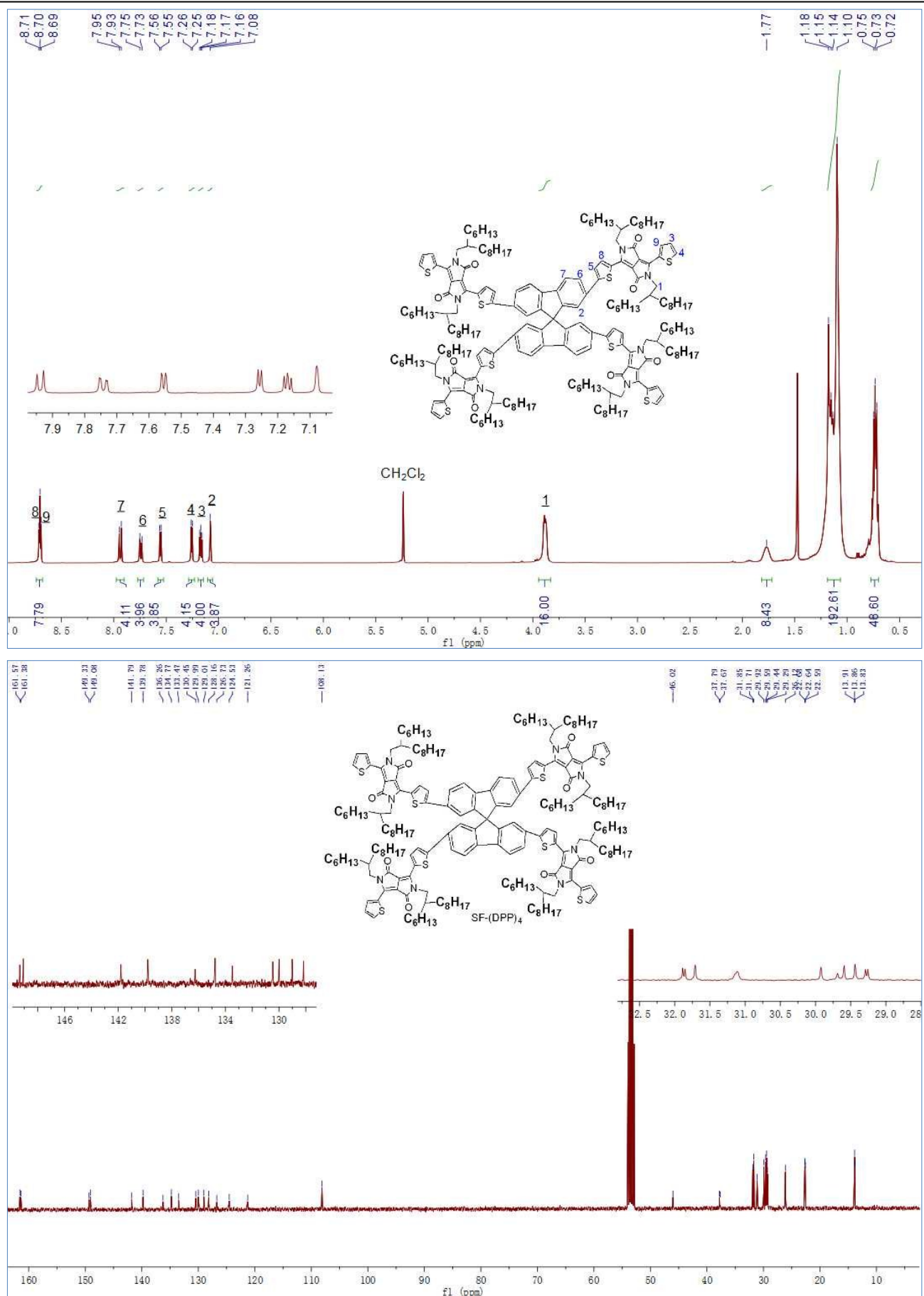


**Fig. S11** The  $^1\text{H}$  and  $^{13}\text{C}$  NMR spectra of DPP-DPP-DPP in  $\text{CDCl}_3$ .

**Fig. S12** The <sup>1</sup>H and <sup>13</sup>C NMR spectra of TB-(DPP)<sub>3</sub> in  $\text{CDCl}_3$ .

**Fig. S13** The <sup>1</sup>H and <sup>13</sup>C NMR spectra of Py-(DPP)<sub>4</sub> in  $\text{CD}_2\text{Cl}_2$ .

**Fig. S14** The <sup>1</sup>H and <sup>13</sup>C NMR spectra of TBE-(DPP)<sub>4</sub> in CD<sub>2</sub>Cl<sub>2</sub> and in CDCl<sub>3</sub>, respectively.

**Fig. S15** The <sup>1</sup>H and <sup>13</sup>C NMR spectra of SF-(DPP)<sub>4</sub> in  $\text{CD}_2\text{Cl}_2$ .

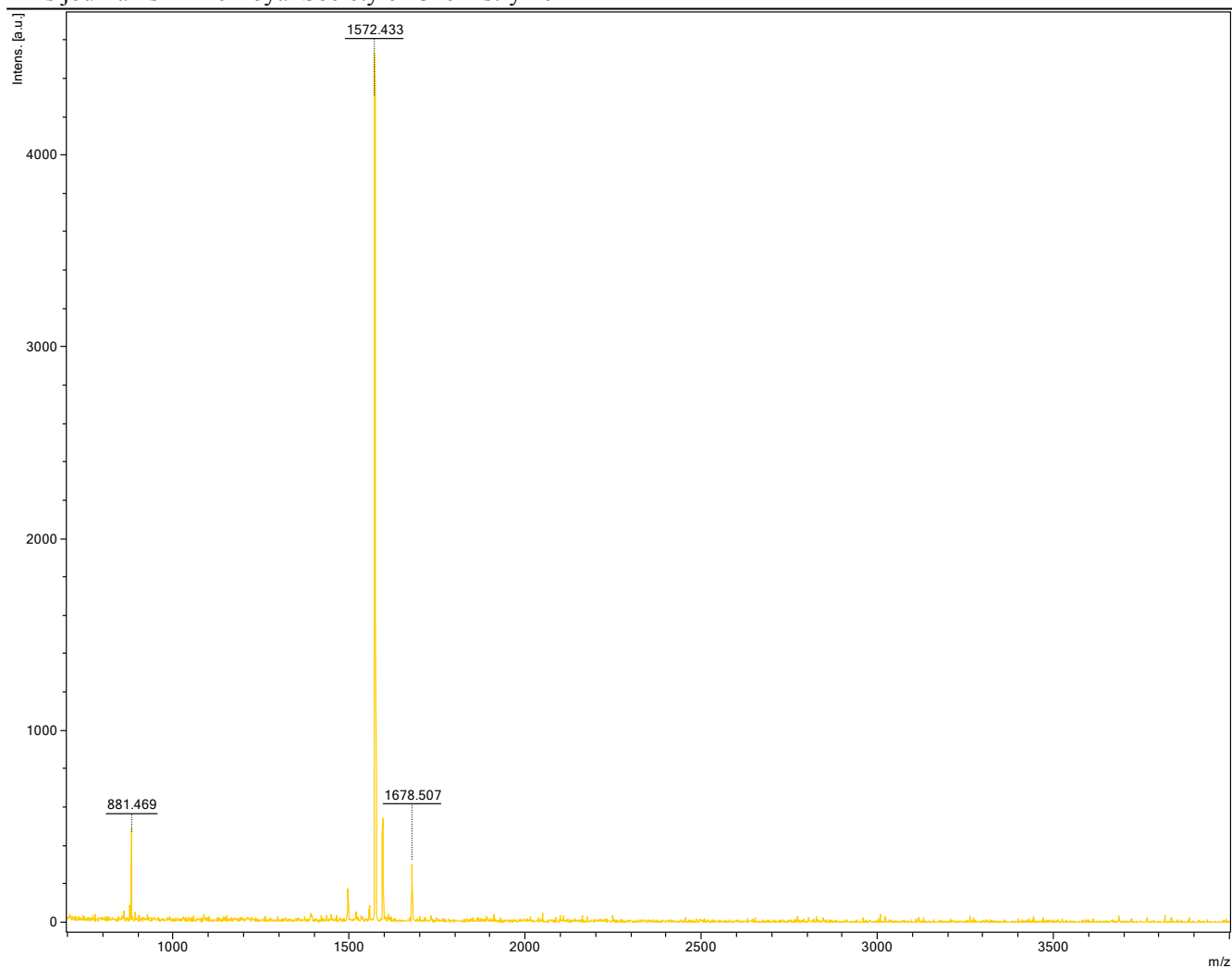


**Fig. S16** The MALDI-TOF MS spectrum of *p*-B-(DPP)<sub>2</sub>, calcd. 1572.51, found 1572.43.

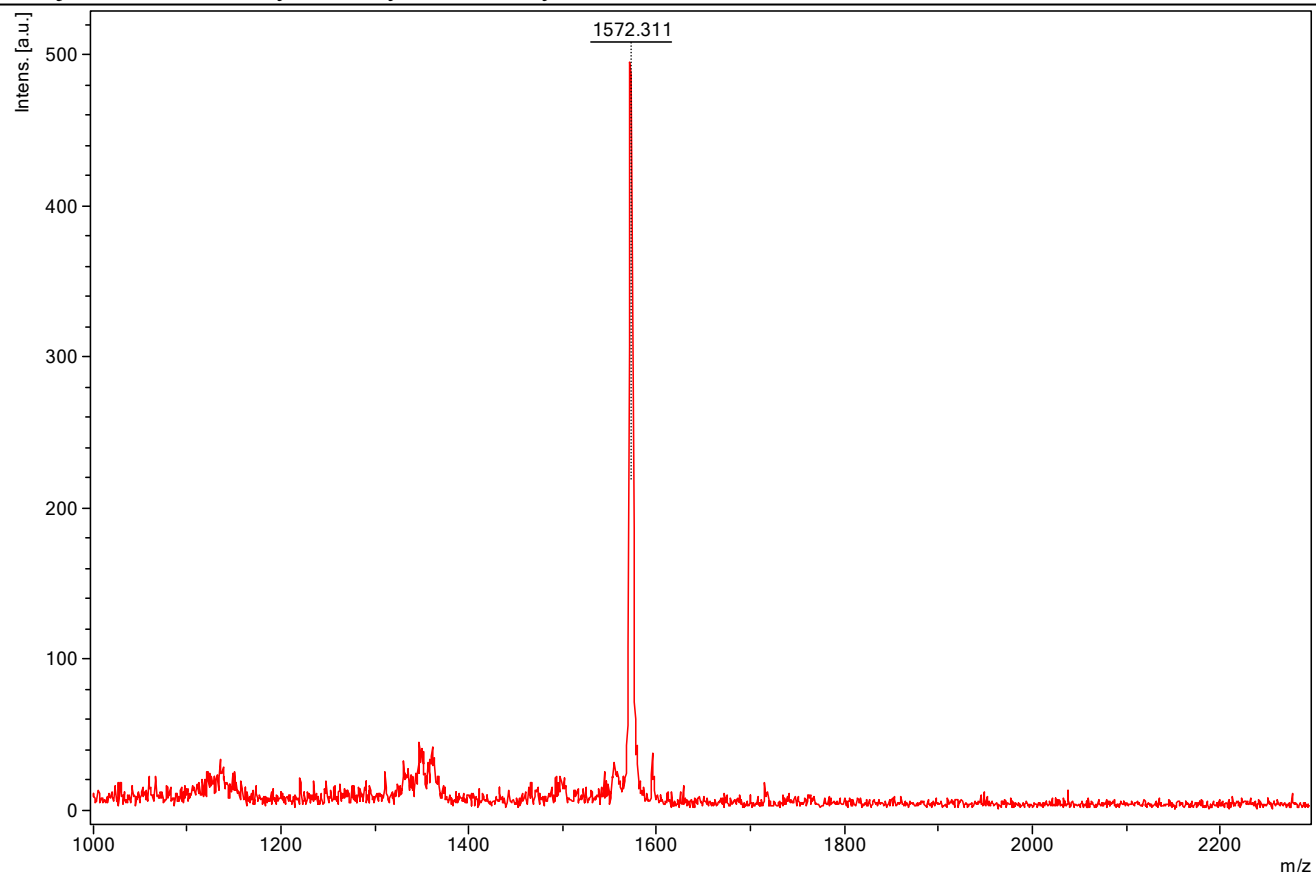


**Fig. S17** The MALDI-TOF MS spectrum of *m*-B-(DPP)<sub>2</sub>, calcd. 1572.51, found 1572.31.

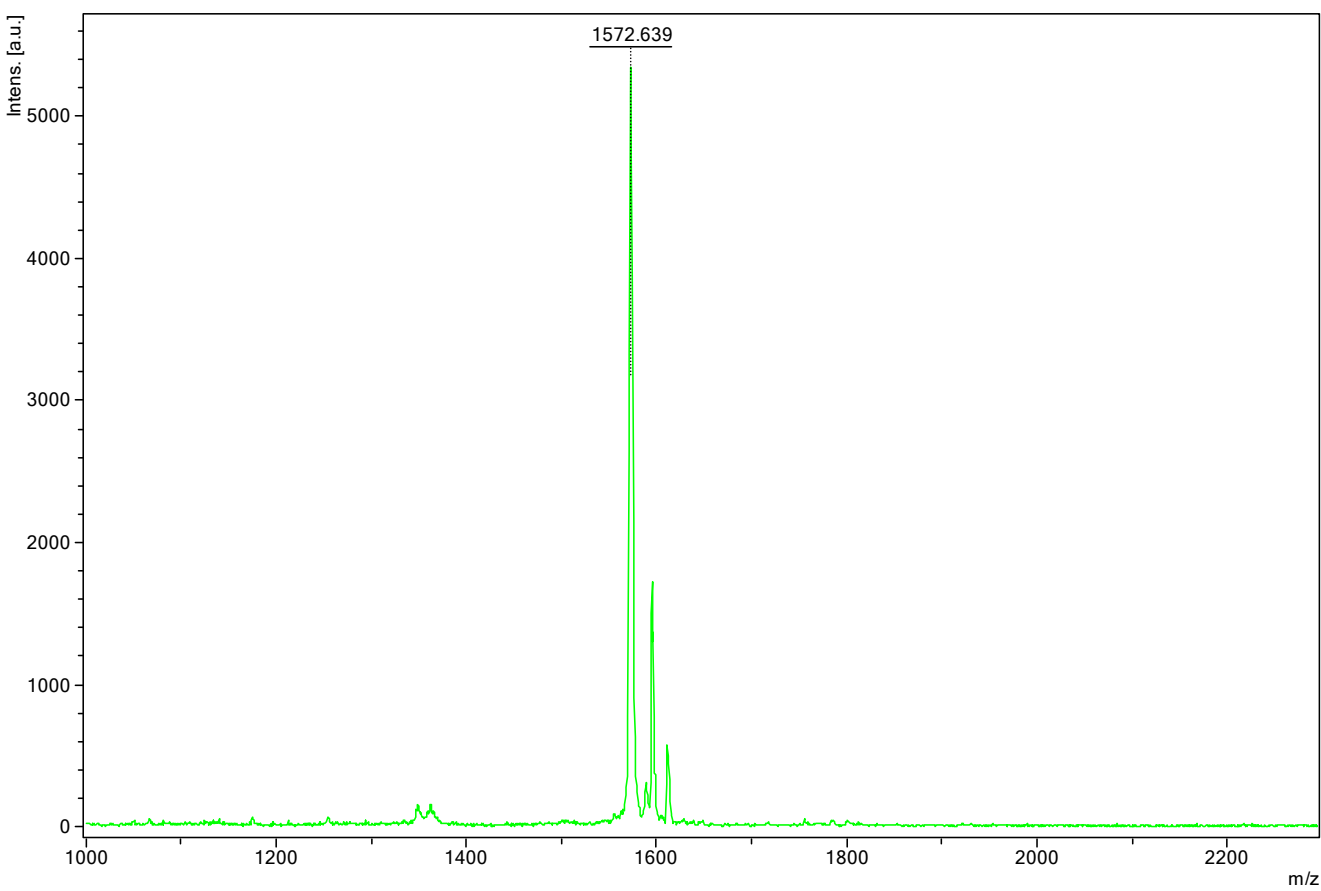


**Fig. S18** The MALDI-TOF MS spectrum of *o*-B-(DPP)<sub>2</sub>, calcd. 1572.51, found 1572.64.

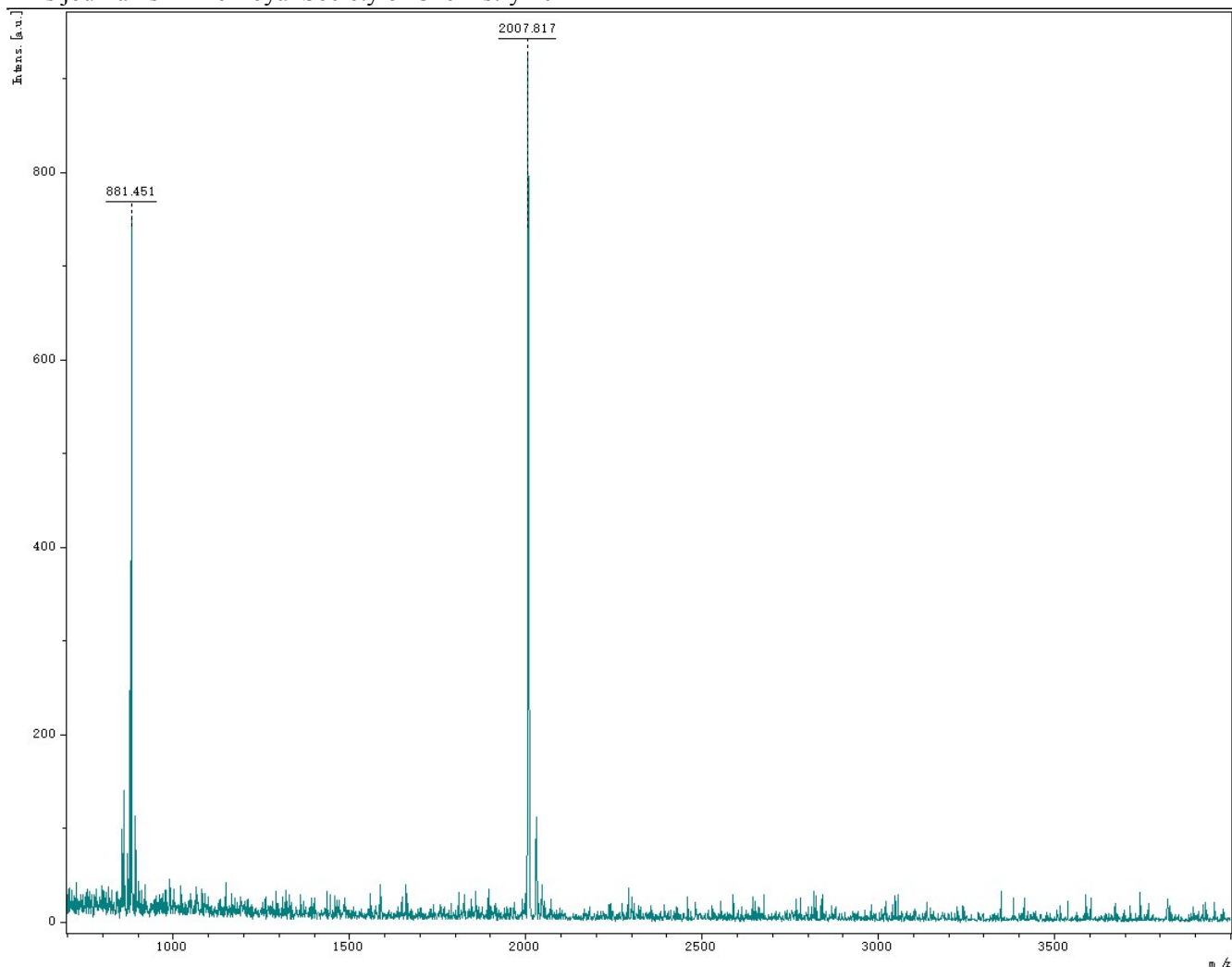


**Fig. S19** The MALDI-TOF MS spectrum of **DPP-DPP-DPP**, calcd. 2007.13, found 2007.82.

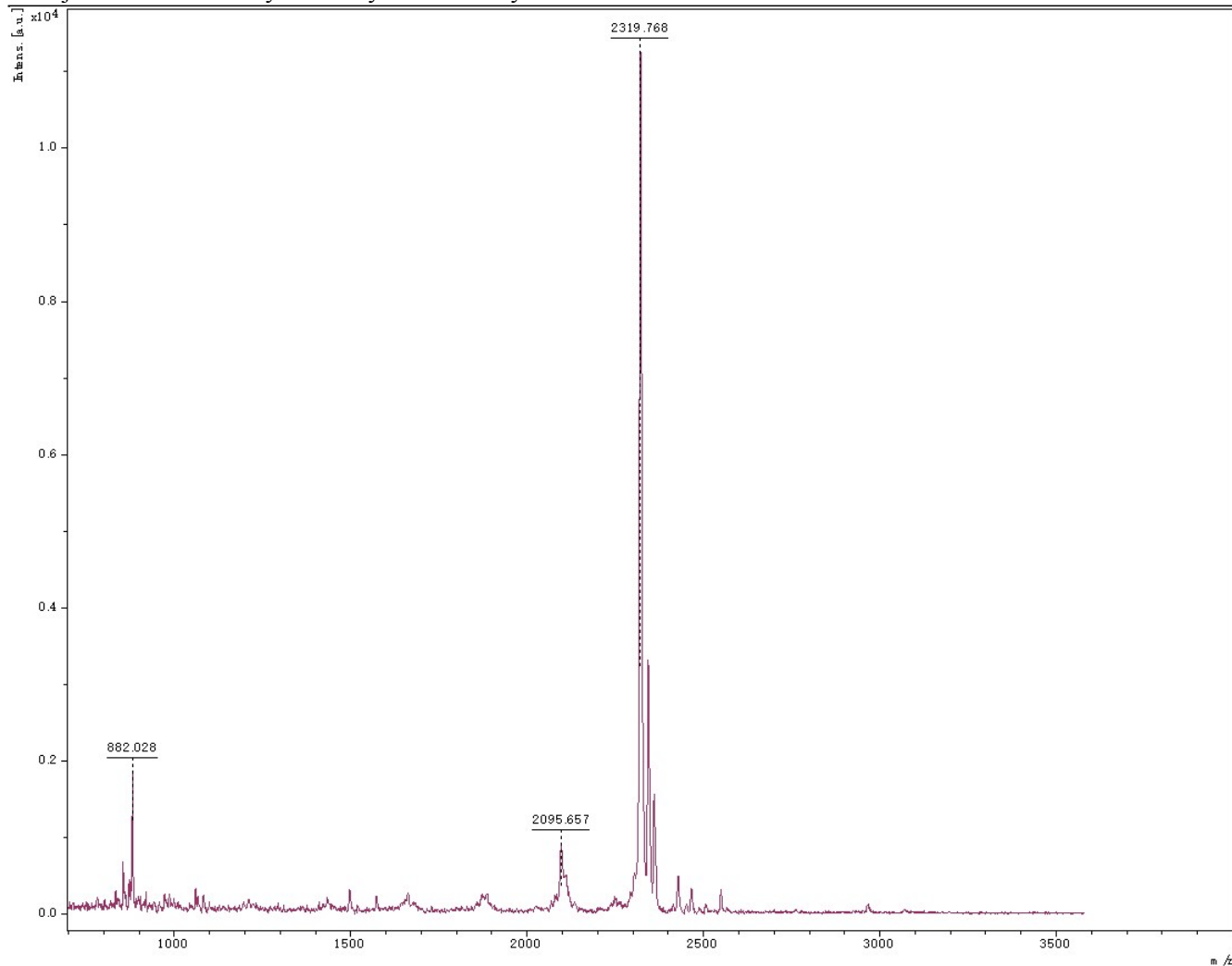


**Fig. S20** The MALDI-TOF MS spectrum of **TB-(DPP)<sub>3</sub>**, calcd. 2319.71, found 2319.77.

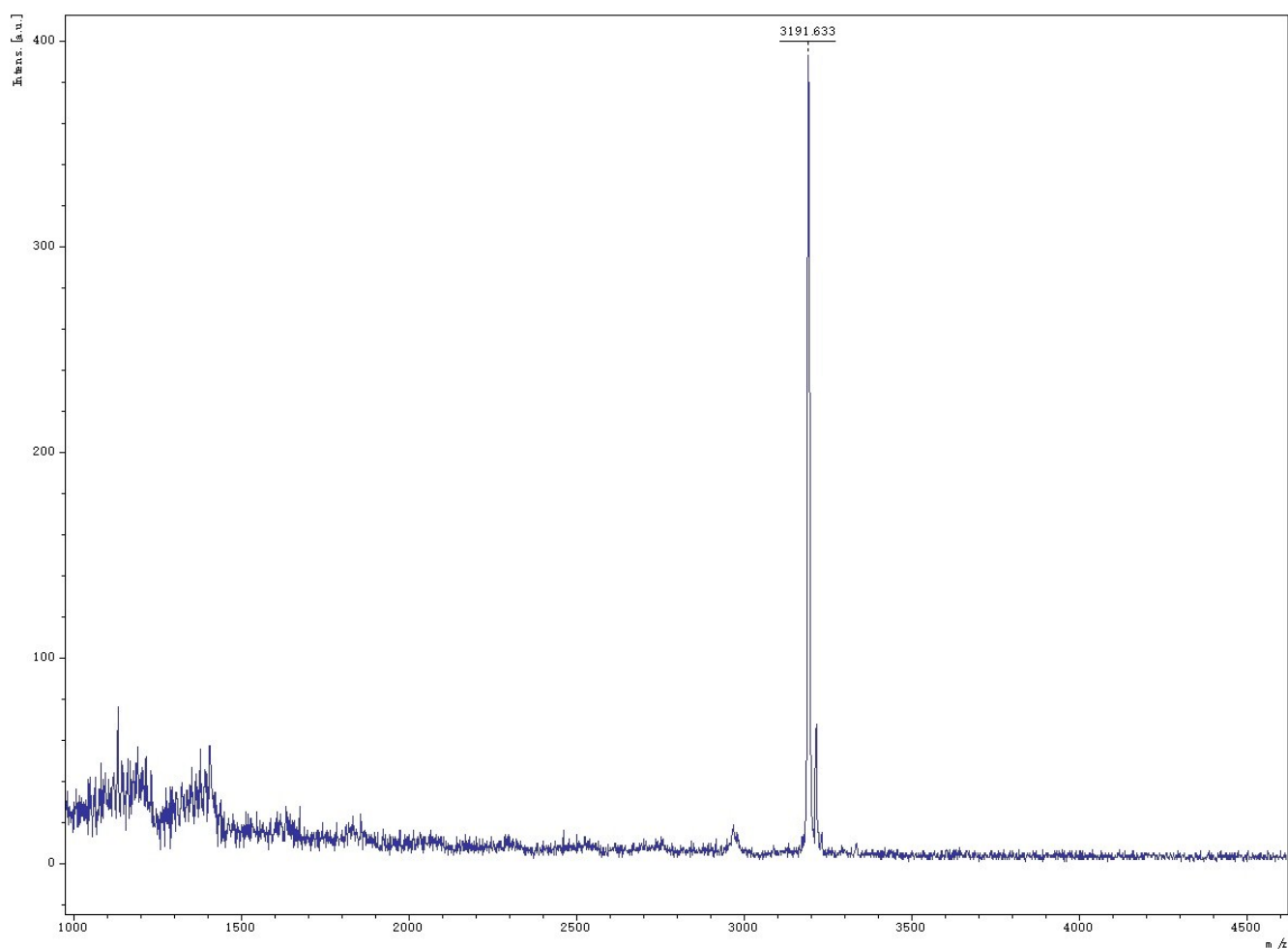


**Fig. S21** The MALDI-TOF MS spectrum of **Py-(DPP)<sub>4</sub>**, calcd. 3191.05, found 3191.63.

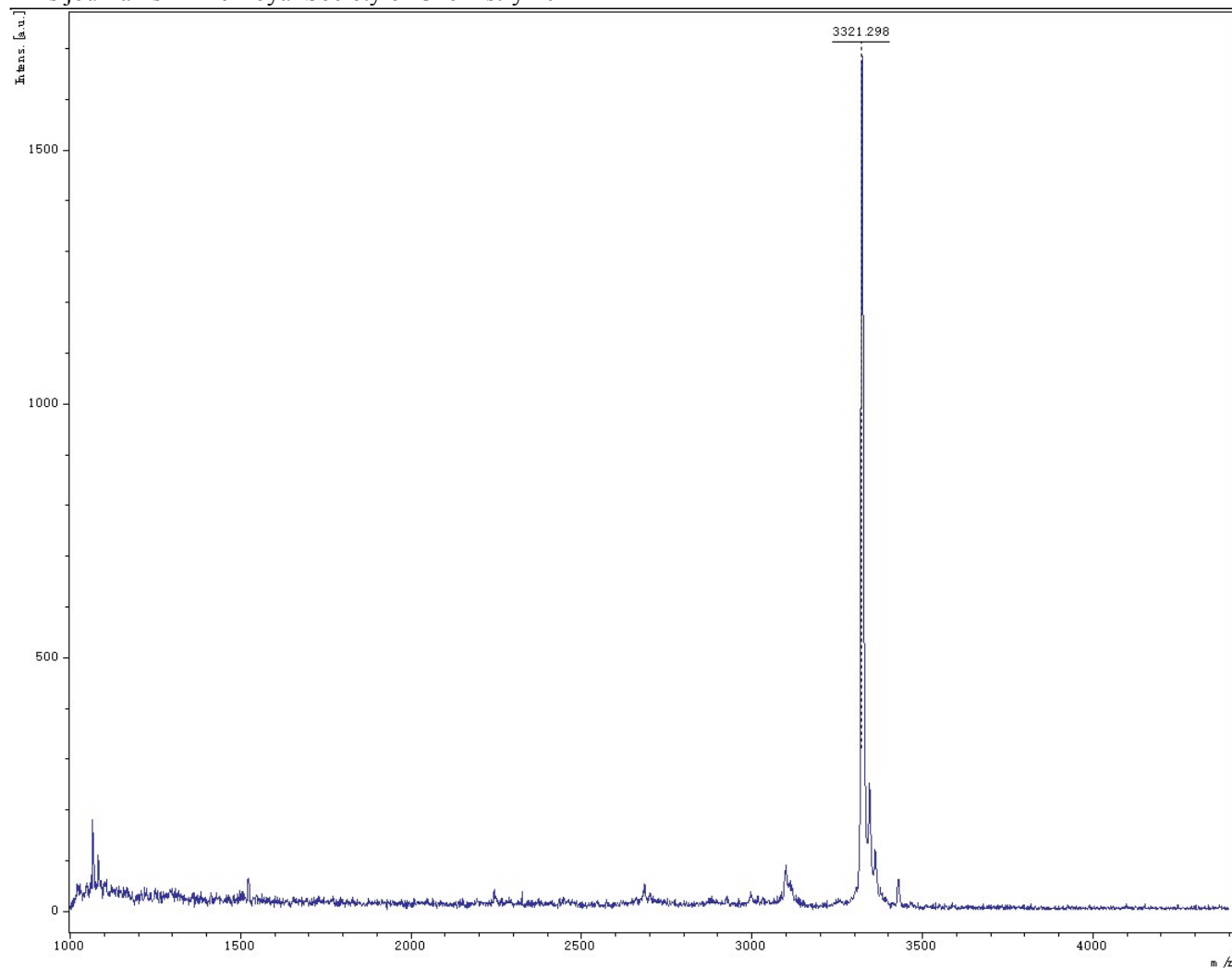


**Fig. S22** The MALDI-TOF MS spectrum of TBE-(DPP)<sub>4</sub>, calcd. 3321.34, found 3321.30.

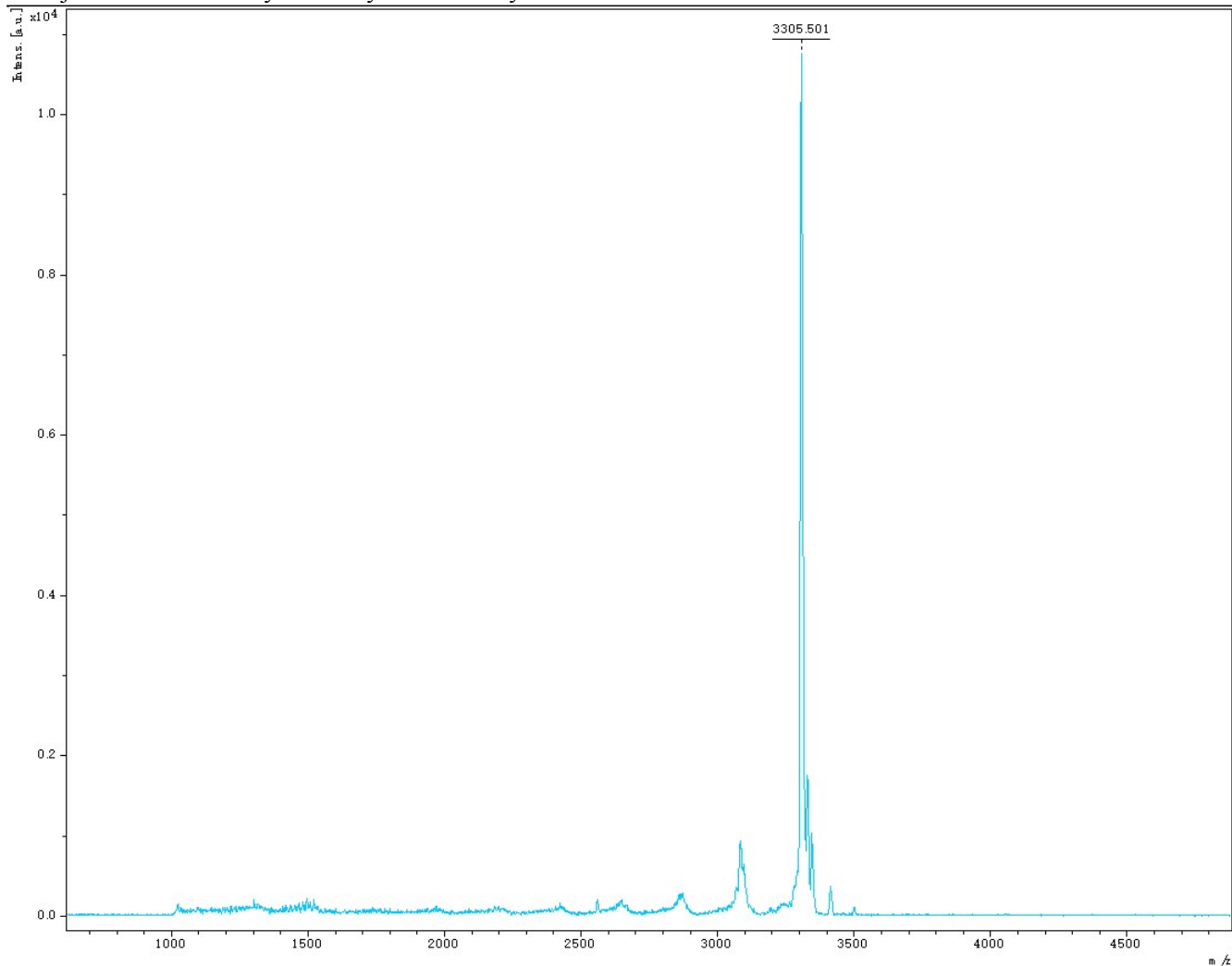


**Fig. S23** The MALDI-TOF MS spectrum of SF-(DPP)<sub>4</sub>, calcd. 3305.20, found 3305.50.